Acta Histochemica 124 (2022) 151840

Contents lists available at ScienceDirect

Acta Histochemica

journal homepage: www.elsevier.com/locate/acthis

Early development of the pulmonary vascular system: An anatomical and histochemical reinvestigation of the pulmonary venous return development in mice

Shizuka Abe [a,*], Aki Murashima [a,*], Eiji Kimura [a], Masatsugu Ema [b], Jiro Hitomi [a]

[a] Department of Anatomy, School of Medicine, Iwate Medical University, Iwate 0283694, Japan
[b] Research Center for Animal Life Science, Shiga University of Medical Science, Shiga 5202192, Japan

ARTICLE INFO

Keywords:
Pulmonary vein
Endomucin
CD31
Flk1
Pulmonary venous return
Mouse embryo

ABSTRACT

Pulmonary venous return development establishes the fetal circulation and is critical for the formation of pulmonary circulation independent of systemic circulation at birth. Anomalous returns lead to inappropriate drainage of blood flow, sometimes resulting in neonatal cyanosis and cardiac failure. While many classical studies have discussed the anatomical features of the pulmonary venous system development, the cellular dynamics of the endothelia based on the molecular marker expression remain unknown. In the present study, we examined the expression of several endothelial markers during early pulmonary vascular system development of murine embryos. We show that Endomucin and CD31 are expressed early in endothelial cells of the splanchnic plexus, which is the precursor of the pulmonary vascular system. Three-dimensional analyses of the expression patterns revealed the spatiotemporal modification of the venous returns to systemic venous systems or sinoatrial canal during the formation of the pulmonary plexus. We herein report the results of spatiotemporal analyses of the early pulmonary venous system development with histochemistry as well as a delineation of the anatomical features of the tentative drainage pathways.

1. Introduction

Anomalous pulmonary venous return (APVR) is a congenital heart defect in which pulmonary veins (PVs) that normally return oxygenated blood to the left atrium are malpositioned and anomalously connect to the systemic venous circulation. It is life-threatening if all four PVs are affected, a condition known as total anomalous pulmonary venous return (TAPVR). To explain the pathology of APVR, it is necessary to understand the normal development of the pulmonary vascular system, which is drastically modified through the coordinated development of the cardiopulmonary organ and systemic venous system.

In normal development, the respiratory system is formed from the primitive foregut and their common vascular system, called the splanchnic plexus, which drains into the cardinal and umbilicovitelline venous systems. As the lung buds develop, the anterior portion of the splanchnic plexus differentiates into the primitive pulmonary vascular plexus. At the same time, the heart tube is formed, and the dorsal mesocardium, which originates from part of the splanchnic mesoderm, connects the primitive heart and lung mesenchyme. Subsequently, primordial evagination of the endocardium from the sinoatrial region (pulmonary pit) (Webb et al., 1998) is observed, resulting in the formation of the primitive PV in the dorsal mesocardium osculating the primitive pulmonary vascular plexus. As the connection is made, the primitive pulmonary vascular system gradually separates from the splanchnic plexus. Although numerous classical but careful examinations on the pulmonary vessel development have been conducted, the precise cellular mechanism underlying PV formation with regard to the coordinated development of the drainage pathways has not been represented adequately (Auër, 1948; Blom et al., 2001; Brown, 1913; Butler, 1952; DeRuiter et al., 1993; Shaner, 1961; Tasaka et al., 1996; Webb et al., 1998).

To study the development of vascular systems, endothelial cell markers, including CD31, CD34 and Flk-1/Vegfr2, have been used (Degenhardt et al., 2013; Peng et al., 2013; Pusztaszeri et al., 2006; Yamamoto et al., 2007). In the transgenic mouse models that show the APVR phenotype, it was demonstrated that the PV originated partially in the dorsal mesocardium and pulmonary vessels. However, the anatomical processes underlying the establishment of the vascular network,

* Corresponding authors.
E-mail addresses: skamei@iwate-med.ac.jp (S. Abe), amura@iwate-med.ac.jp (A. Murashima).

https://doi.org/10.1016/j.acthis.2021.151840
Received 12 February 2021; Received in revised form 27 December 2021; Accepted 29 December 2021
Available online 15 January 2022

especially the development of the primitive pulmonary vascular plexus and PVs in correlation with the peripheral and/or central circulation system, have not been clarified systematically.

In the present study, we investigated the developmental process of pulmonary vasculature utilizing endothelial cell markers, Endomucin, CD31, CD34 and Flk1. Fluorescent confocal microscopic analyses and three-dimensional (3D) analyses consolidated the classical observation that the pulmonary vascular plexus arose from the splanchnic plexus, and its drainage was demonstrated to change drastically during the formation of the PV. Furthermore, we demonstrated a characteristic expression profile of the endothelial cell markers in early splanchnic plexus which delineates the temporal peripheral and central venous return pathways.

2. Materials and methods

2.1. Mice

Wild-type ICR mice and *Flk1-GFP* BAC transgenic (*Flk1-GFP*) (Ishitobi et al., 2010) mice were utilized for this study. Two females were housed overnight with a male, and the presence of a vaginal plug the following morning was considered evidence of copulation. Noon on the day on which the vaginal plug appeared was designated as embryonic day (E) 0.5. Embryos were collected between E8.5 and E16.5 and fixed for at least 2 h and up to overnight in 4% paraformaldehyde with phosphate-buffered saline (PBS). After fixation, embryos were washed in PBS containing 0.1% Tween 20 and dehydrated through a series of methanol washes (25%, 50%, 75%, 100%). These samples were stored at − 20 °C until they were used for immunofluorescence or immunohistochemistry. For this study, embryos were collected from more than two different ICR or *Flk1-GFP* mothers, at each stage. Forty-two ICR and 16 *Flk1-GFP* female mice were sacrificed.

All experimental procedures and protocols were approved by the Committees on Animal Research at Iwate Medical University, and the experiments were carried out in accordance with the approved guidelines.

2.2. Whole-mount immunofluorescence

Before staining, the lungs, hearts and vessels with these organs were dissected from E11.5 and older embryos. Whole embryos were used for E10.5 and younger specimens. They were rehydrated, and the endogenous peroxidase activity was quenched with 3% H_2O_2 (this process was omitted for *Flk1-GFP* mouse staining). Specimens were washed 5 times with 1% triton-X in PBS, and non-specific antibody binding was blocked by pre-incubating specimens in 10% fetal bovine serum (FBS). Specimens from wild-type ICR and *Flk1-GFP* mice were then stained for 3 days with goat anti-CD31 antibody (AF3628; R&D Systems, Minneapolis, MN, USA, 1:50 dilution), rabbit anti-CD34 antibody (ab81289; Abcam, Cambridge, UK, 1:500 dilution) and rat anti-Endomucin (Emcn) antibody (sc-65495; Santa Cruz, Dallas, TX, USA, 1:500 dilution). Specimens were washed and incubated with anti-rat Alexa Fluor 594 and anti-goat Alexa Fluor 647 (A21209, A21447; Thermo Fisher Scientific, 1:200 dilution) for CD31/Emcn double staining. Anti-CD34 antibody was detected by staining for 3 days with anti-rabbit HRP secondary antibody (A10547; Thermo Fisher Scientific, Waltham, MA, USA, 1:200 dilution) followed by incubation with a TSA Fluorescence System (PerkinElmer, Waltham, MA, USA) for 1 h. Anti-rat Alexa 594 (A11007, Thermo Fisher Scientific, 1:200 dilution) was applied for the Emcn staining with anti-CD34 antibody and Emcn detection in *Flk1-GFP* embryos. Specimens were then stained with Hoechst 33342 (Sigma-Aldrich, Osaka, Japan) for 1 h, soaked in 50% Tissue-Cleaning Reagent CUBIC-R+ [for animals] (CUBIC-R+) (T3741; Tokyo Chemical Industry, Tokyo, Japan) overnight and replaced by 100% CUBIC-R+ (Hasegawa et al., 2019). As a negative control, embryos were stained without each primary antibody to assert their specificities (Fig. 4M). More than Two embryos containing distinct littermates were analyzed for each developmental stage of the experiment (Supplemental Table 1). Confocal laser scanning microscope LSM510 (Zeiss, Oberkochen, Germany) and A1R (Nikon, Tokyo, Japan) were used to take Z-stack images. Serial images and projection images (maximum intensity) were obtained and analyzed using the ImageJ software program (National Institute of Health, Bethesda, MD, USA) and Imaris Viewer 9.7.0 software program (Oxford Instruments, Zurich, Switzerland) (Rasband, 1997; Schneider et al., 2012). For the 3D reconstruction, stained vessels were labeled for every slice of the specimens by visual observation and reconstructed using the surfacegen algorithm in the Amira 5.6 software program (Field Electron and Ion Company, Hillsboro, OR, USA). Representative images of the analyzed embryos of each stage are shown in the supplemental movies.

2.3. Immunohistochemistry for paraffin sections

E9.0 to E11.5 embryos were used for immunohistochemistry, as described previously (Murashima, 2011). Embryos were embedded in paraffin and serially sectioned at 6-μm thickness. After deparaffinization and hydration, sections were washed with distilled water and autoclaved at 121 °C for 1 min in citrate buffer to activate antigens. Endogenous peroxidase activity was quenched with 3% H_2O_2. Non-specific antibody binding was blocked by pre-incubation of specimens in 1% FBS/PBS. Sections were stained for 1 h with rat anti-Emcn antibody (sc-65495; Santa Cruz Biotechnology, 1:500 dilution) at room temperature. Primary antibody was detected by staining for 30 min with anti-rat HRP secondary antibody (ab6845; Abcam, 1:200 dilution) followed by incubation with 3. 3'-diaminobenzidine (DAB) (040–27001; Wako, Osaka, Japan) solution for 10–30 min. Sections were washed and nuclear-stained with hematoxylin. Subsequently, sections were dehydrated, permeated and mounted using Malinol (Muto Pure Chemicals, Tokyo, Japan). As a negative control, specimens were stained without primary antibody (data not shown).

3. Results

3.1. Precirculatory stage

At E8.5 (Theiler stage [TS] 13), the primitive heart is divided into a common atrium, which receives blood flow from the right and left horns of sinus venosus (SV), and a common ventricle, which connects to the bulbus cordis. At this stage, the heart, dorsal aorta and systemic veins were detected based on the expression of Emcn, CD31 (Fig. 1A-F) and CD34 (data not shown). Respiratory diverticulum was not observed, and the splanchnic plexus was not detected by either Emcn, CD31 (Supplemental video 1) or CD34 antibodies (data not shown). Flk1 is another marker of endothelial cells during vessel formation. Similar to the expression of Emcn and CD31, *Flk1-GFP* embryos showed GFP expression in the heart and dorsal aorta but not in the splanchnic plexus (data not shown).

At E9.0 (TS 14), the looped heart tube contains four anatomical segments: a primitive atrium, atrioventricular canal, ventricle and outflow tract (Fig. 2A-C). Primitive circulation has been established, and the inflow tract receives umbilical veins, vitelline veins and common cardinal veins, which form the junctions of the anterior and posterior cardinal veins, at horns of SV (Fig. 2A-C, Supplemental video 2–4) (Brune et al., 1999; Savolainen et al., 2009). The common atrium was formed dorsocaudally to the ventricles interposed between the SV and the outflow tract (Fig. 2A-C). The thickening of the epithelium as a primary morphological feature of the laryngotracheal groove was seen at the ventral side of the foregut (Supplemental video 2–4, Theiler, 1989). The expression of Emcn, CD31 and CD34 was detected in the dorsal aorta, pharyngeal arch arteries and most of the endocardium including inflow and outflow tract (Fig. 2A and B). Vitelline veins and cardinal veins are also responsive to these antibodies (Fig. 2A and B). The cardiovascular structures, such as the common atrium, ventricle, SV

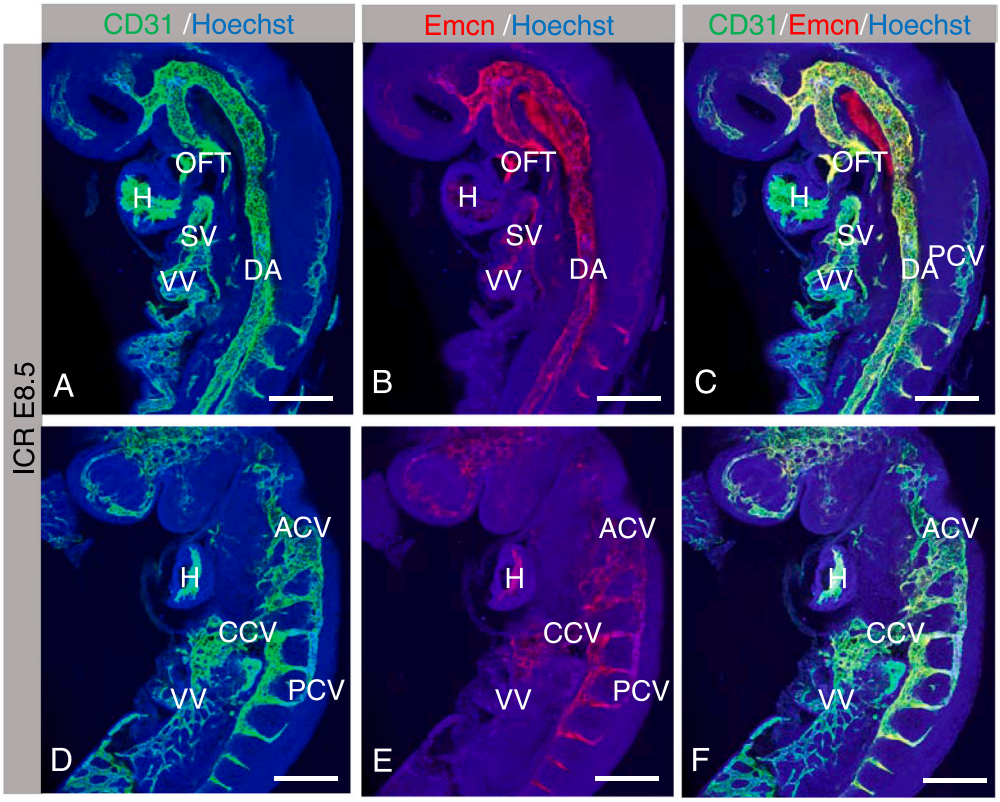

Fig. 1. Morphology and vascular images of the whole ICR embryo at E8.5 (A-F). Projection images showing the connection between the heart tube and dorsal aorta (A-C), and the cardinal vein (D-F) detected by Emcn and CD31 antibodies. No signs of the splanchnic plexus were detected at this stage. A, common atrium; V, common ventricle; H, heart tube; OFT, outflow tract; DA, dorsal aorta; ACV, anterior cardinal vein; CCV, common cardinal vein; PCV, posterior cardinal vein; VV, vitelline vein. Bar = 300 μm.

and inflow and outflow tract, were also identified by *Flk1-GFP* (Fig. 2C). The splanchnic plexus formed dorsal to the primitive atrium and SV were clearly detected and double-positive for Emcn and CD31 (5/7) (Fig. 2E-G). While one out of five plexuses detected by Emcn was barely detectable by CD34 (Fig. 2I-K). The splanchnic plexus detected by Emcn was also positive for GFP in the *Flk1-GFP* mice (2/4) (Fig. 2L-N). The splanchnic plexuses were connected to the dorsal wall of sinoatrial segment and SV at its cranial and caudal sight (Fig. 2E-H, R yellow and red arrowhead). Either sights line midline and detected by all the marker molecules investigated including CD34 (Fig. 2E-N, Supplemental video 2–4). A number of connections between the plexus and dorsal aorta were identified by all the marker molecules investigated (Fig. 2E-G, I-N, P white arrow). These markers detected several vessels of the plexus linked with vitelline vein and common cardinal veins (Fig. 2H, S white arrows, Supplemental video 2–4). Based on these results, the splanchnic plexus primarily forms two possible drainage pathways to the atrium. One is the route that directly returns to the atrium after perfusion of the gastrorespiratory organ, while the other pathways return to the atrium via cardinal veins, vitelline veins and SV.

Histological analyses using Emcn antibody revealed that the endocardial cells of the sinoatrial region sprouting to the dorsal mesentery were the first feature of the primitive PV formation which was confirmed in the wholemount immunostaining (Fig. 2E-G and U, yellow arrowhead). This histological observation was previously described as a "pulmonary pit" at E9.5 with alcian blue (pH 2.5) and nuclear fast red or Masson's trichrome staining (Tasaka et al., 1996; Webb et al., 1998). The strand of the primitive PV and most of the splanchnic plexus did not show canalization at this time point (Fig. 2E, K, N and U). Three-dimensional reconstruction of Emcn-stained specimens showed that the splanchnic plexus had junctions with the dorsal aorta, SV and sinoatrial segment (Fig. 2P and R). Pulmonary arteries and sixth pharyngeal arch arteries were not detected at this stage. These results suggest that the shared pathway for the gastric and respiratory tract is prepared prior to its blood supply shunting the systemic arterial circulation into systemic venous tributaries, such as the cardinal veins, vitelline veins and umbilical veins.

3.2. Peripheral and intermediate stages

At E9.5 (TS 15), there were no fundamental changes in the primitive heart (Fig. 3A and B). The respiratory diverticulum was recognized as a thickening of the epithelium on the ventral side of the foregut, as observed in the previous stage, and the groove gradually deepened and separated from the digestive tract. The cranial part of the splanchnic plexus expanded and increased in complexity compared to the previous stage (Fig. 3C-H compared to Fig. 2E-G). The plexus expressed Emcn (19/19), CD31 (9/9) and CD34 (6/6) in all embryos investigated. All *Flk1-GFP* embryos showed GFP expression together with Emcn in the splanchnic plexus (4/4) (data not shown). The dorsal aorta, SV and most of the systemic tributaries were positive for Emcn, CD31, CD34 and Flk1 throughout the analyses until E11.5 (Fig. 3A, B and L, Fig. 5A-F). The connections between the splanchnic plexus and sinoatrial segment was observed by Emcn (15/15), CD31 (9/9) and CD34 (6/6). (Fig. 3C-H and M-O, yellow arrowhead). The connections between the splanchnic plexus and dorsal aorta were confirmed by Emcn, CD31 and CD34 antibodies at this stage (Fig. 3C-E, J, K and M-O, white arrow). Caudal part of the plexus (hereafter we call gastrointestinal plexus) osculates to the SV and vitelline veins (Fig. 3I, J), while cranial part of the splanchnic plexus, which contributes to the primitive pulmonary plexus, connects to the common cardinal vein with Emcn/CD31 double-positive endothelia (Fig. 3F and G). These connections were also detected in CD34 (Fig. 3M-O, Supplemental video 6) and *Flk1-GFP* mice (data not shown.).

At E10.0 (TS 16), the left and right components of the common atrial chamber are distinguishable by the emergence of the spina vestibuli, also called the dorsal mesenchymal protrusion (His, 1880; Tasaka et al., 1996; Wessels et al., 2000), and the atria located at the dorso-anterior side of the ventricles (Fig. 4A-C, Supplemental video 7). Bilateral lung buds were clearly identified at the ventral side of the foregut in the present study (Fig. 4A-G). The splanchnic plexus was distinguishable by the cranial pulmonary plexus surrounding the lung buds and caudal

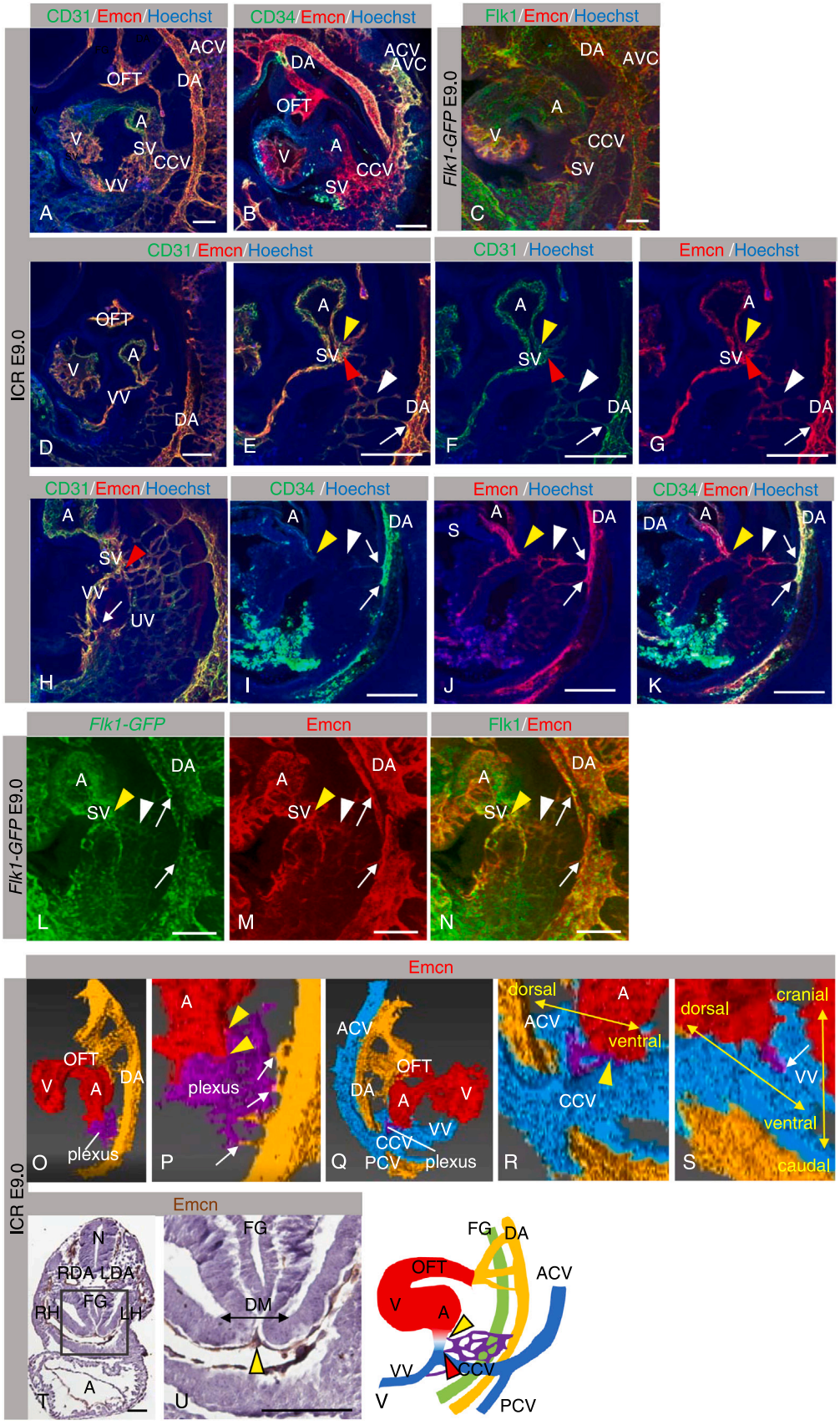

Fig. 2. Projection images showing the morphology of the vasculature in ICR (A, B, D-K) and Flk1-GFP (C, L-N) embryos at E9.0. Major vessels, including the inflow tract, detected by all endothelial markers (A-C). Low- (D) and high-magnification images (E-N) showing the connections between the plexus and sinoatrial region, dorsal aorta or vitelline veins detected by Emcn and CD31 (D-H), CD34 (I-K) or Flk1-GFP (L-N). E-G and H show different planes of projection which were obtained from distinct embryos. CD34 expression was less prominent in the splanchnic plexus compared to Emcn (I-K). An Flk1-GFP embryo stained by Emcn antibody showing the splanchnic plexus, dorsal aorta and venous pole of the heart (L-N). Three-dimensional images of the pathways linking the splanchnic plexus (purple) reconstructed based on Emcn staining (O-S). P and R show enlarged views of O and Q, respectively. S shows a rotated view of R. Histological analyses of the Emcn expression showing the pulmonary pit in the sinoatrial region (U, yellow arrowheads, U is the axial view). U shows enlarged view of T. Schematic diagram showing the topological structure of the vascular system and foregut analyzed (V). Splanchnic plexus is connected to sinoatrial region, SV and systemic vessels (V). A, common atrium; V, common ventricle; DA, dorsal aorta; OFT, outflow tract; VV, vitelline vein; ACV, anterior cardinal vein; CCV, common cardinal vein; PCV, posterior cardinal vein; SV, sinus venosus; N, neural tube; FG, foregut; DM, dorsal mesocardium; white arrowheads, splanchnic plexus; yellow arrowheads, connections between the sinoatrial region and the splanchnic plexus; red arrowhead, connection between the SV and caudal part of splanchnic plexus; white arrow, connections between the systemic vessels and the plexus. Bar = 200 μm (A-N) and 100 μm (T and U).

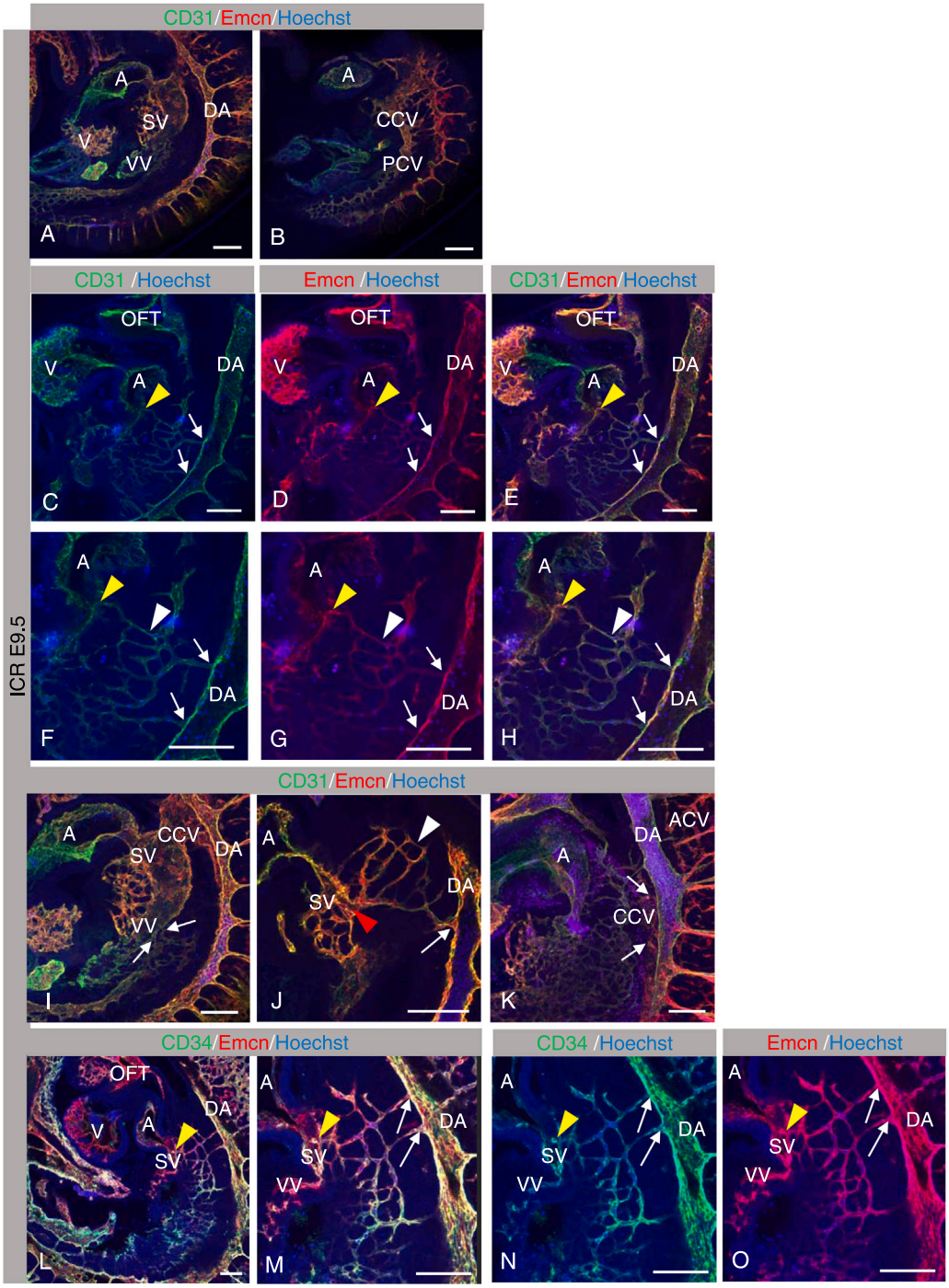

Fig. 3. Projection images showing the morphology of the vasculature in ICR embryos at E9.5. Two different planes of the projection are shown (A and B). Double-stained embryos by Emcn and CD31 (A-K) or CD34 (L-O) antibodies are shown. Enlarged images of C-E are shown in F-H. The connections between the splanchnic plexus and the vitelline vein (I), the SV (J) or the common cardinal vein (K) are shown in different projection planes which were obtained from different embryos. M-O show enlarged and individual staining images of L. A, common atrium; V, common ventricle; DA, dorsal aorta; OFT, outflow tract; VV, vitelline vein; ACV, anterior cardinal vein; CCV, common cardinal vein; PCV, posterior cardinal vein; SV, sinus venosus; yellow arrowheads, connections between the sinoatrial segment and the splanchnic plexus; white arrowheads, splanchnic plexus; white arrow, connections between the systemic vessels and the plexus. Bar = 200 μm.

gastrointestinal plexus, in which the Emcn, CD31 (Fig. 4A-F), CD34 and Flk1-GFP (data not shown) expressions were observed. The connections linking the pulmonary plexus and the sinoatrial region were detected using all of the endothelial markers applied in this study (Fig. 4A-C, yellow arrowhead, data of CD34 and Flk1-GFP not shown). Immunohistochemistry of Emcn with paraffin sections demonstrated that the connection emerging from the pulmonary plexus reached the left part of the common atrium with a canalized structure confirming PV formation (Fig. 4I). The connection between the splanchnic plexus and SV observed in the previous stage extended more caudally and thickened, contributing to the venous return of the digestive system (Fig. 4D, red arrowhead). At this stage, very thin sixth pharyngeal arch arteries were observed for the first time in some embryos, expressing both Emcn, CD31 and CD34 (Fig. 4E, data not shown). Pulmonary arteries extending from near the junction of the sixth pharyngeal arch arteries and ventral aorta reached the pulmonary plexus were also positive for all the markers investigated (Fig. 4E, yellow arrow, supplemental video 7, data not shown).

Three-dimensional reconstruction of Emcn-stained specimens showed that the pulmonary plexus flowed into left side of the common atrium and connected to the dorsal aorta and pulmonary arteries (Fig. 4K). It also connected to the anterior cardinal veins in addition to the sinoatrial segment and common cardinal vein, which had already been observed at E9.5 (Fig. 4D, F, Fig. 3H and K). Gastrointestinal plexus, which was not discrete with pulmonary plexus completely, was connected to the vitelline vein (Fig. 4G, white arrows) (van den Berg and

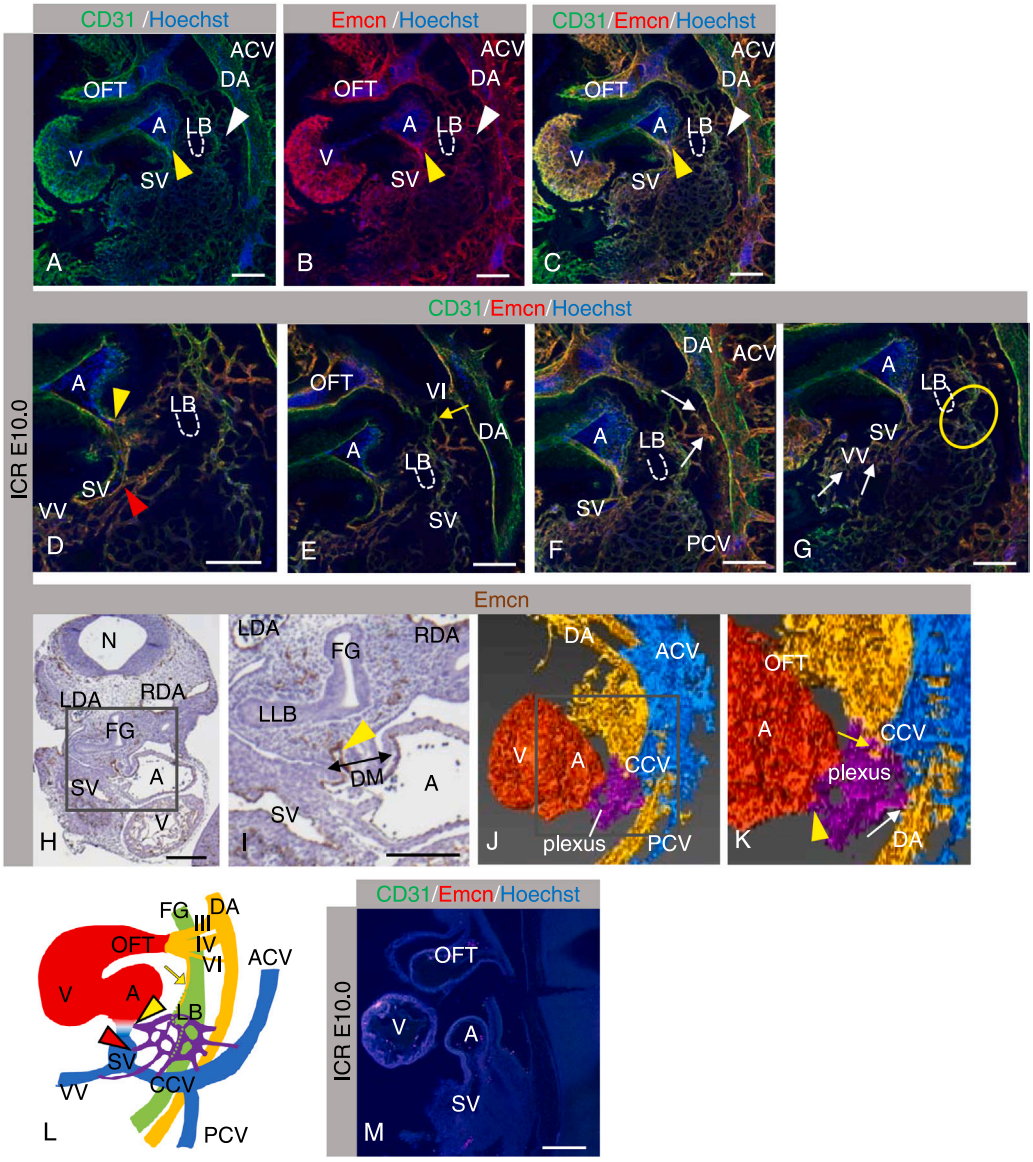

Fig. 4. Projection images showing the morphology of the vasculature in ICR (A-G) embryos at E10.0. Histological images of the Emcn expression (H and I). Three-dimensional images of the pathways linking the splanchnic plexus (purple) reconstructed based on Emcn staining (J and K). Schematic diagram showing the topological structure of the vascular system and foregut/lung bud analyzed (L). Negative control of CD31 and Emcn staining (M). The pulmonary plexus formed around lung buds (A-C white arrowhead) and connected with the sinoatrial region (A-C yellow arrowhead). The caudal part of the splanchnic plexus is connected to the SV (D, red arrowhead). The pulmonary artery (E, yellow arrow) reaches the pulmonary plexus. The connection between the pulmonary plexus and the cardinal veins (F) is shown in the different planes of the projection. The connection between the pulmonary plexus and gastrointestinal plexus is shown (G, yellow circle). I and K show enlarged view of H and J, respectively. Pulmonary artery (yellow arrow) and connections between the pulmonary plexus and the sinoatrial region (yellow arrowhead), the dorsal aorta or common cardinal vein (white arrow) are shown in K. At this stage, the connection between pulmonary plexus and systemic vessels is retained (L). A, common atrium; V, common ventricle; DA, dorsal aorta; DM, dorsal mesocardium; OFT, outflow tract; ACV, anterior cardinal vein; CCV, common cardinal vein; PCV, posterior cardinal vein; SV, sinus venosus; FG, foregut; LLB, left lung bud; N, neural tube; III/IV/VI, 3/4/6th pharyngeal arch artery; yellow arrowheads, connections between the atrium and the pulmonary plexus; red arrowhead, connection between the SV and gastrointestinal plexus; white arrowheads, splanchnic plexus; white arrow, connections between the systemic vessels and the plexus; yellow arrow, pulmonary artery. Bar = 200 μm.

Moorman, 2011). These observations indicated that the blood flow from the pulmonary artery and dorsal aorta interosculated in the plexus and drained through not only the PV but also the systemic venous tributaries at this stage.

3.3. Central drainage stage

At E10.5 (TS17) and thereafter, the chambers of the heart proceeded to differentiate. The atrioventricular cushion separated the atrioventricular canal, and both the ventricle and atrium showed enlargement with a thickened myocardium (supplemental video 8) (de Boer et al., 2012; Wessels et al., 2000). The PV was detected by all the marker molecules and was incorporated into the left atrium following the formation of the venous valve, which divides the sinoatrial region into the atrium and SV at E11.5 (Fig. 5A-C, yellow arrowheads, supplemental video 8). Of note, the caliber of the PV and pulmonary artery became larger than that in the previous stage (Fig. 5A-C; compared to Fig. 4A-E). Numerous junctions to the bronchus were also positive for these markers (Fig. 5A-C, Supplemental video 8). Dense meshwork of the pulmonary plexus was observed dorsocaudally to the atrium surrounding the lung buds, which branched and elongated further (Fig. 5A-C). The osculation between the pulmonary and gastrointestinal plexus remained, while the connections between the pulmonary plexus and systemic veins or dorsal aorta could barely be identified with any markers at E11.5 (Fig. 5D-F, Supplemental video 8). The expression of Emcn, CD31, CD34 and Flk1-GFP was retained in all the vascular system analyzed at E11.5 (supplemental video 8, data not shown). These findings suggest that the central and peripheral pulmonary returns are integrated immediately after the intermediate stage, and the PV develops further following the coordinated development of the four separate chambers of the heart and pulmonary organs.

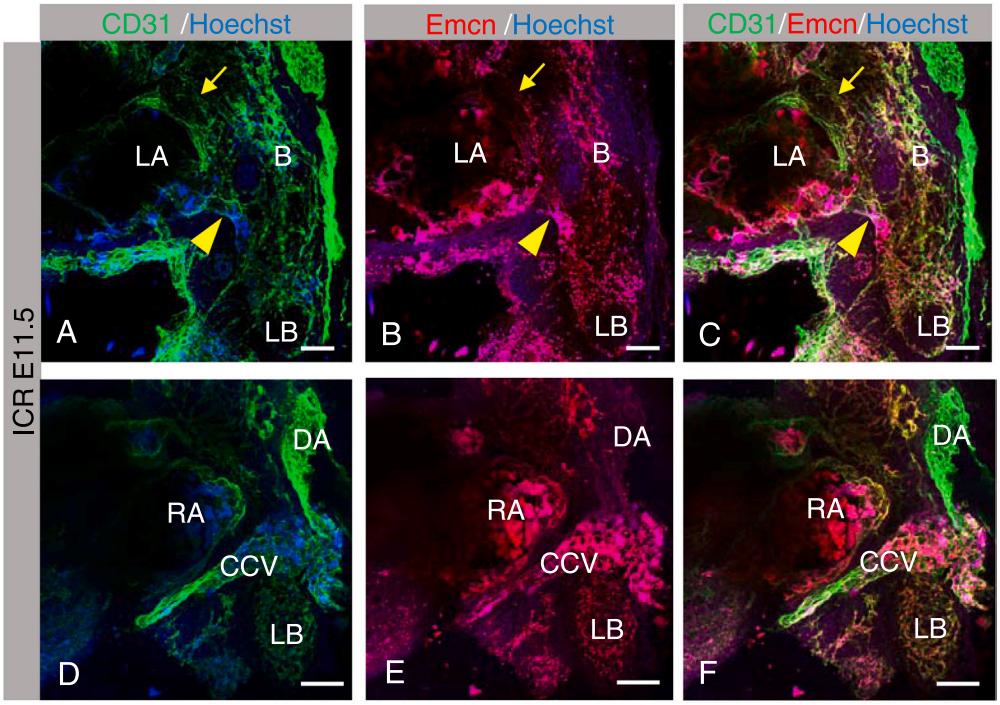

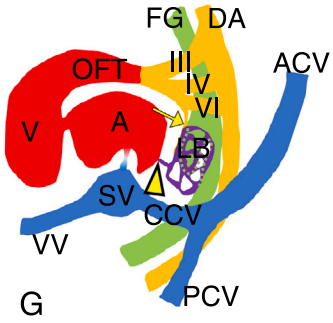

Fig. 5. Projection images showing the morphology of the vasculature in ICR embryos at E11.5 (A-F). Schematic diagram showing the topological structure of the vascular system and foregut/lung bud analyzed (G). Two different planes of the projection are shown (A-C and D-F). The connections between the pulmonary plexus and the systemic veins or dorsal aorta were not detected (D-F). LA, left atrium; DA, dorsal aorta; OFT, outflow tract; ACV, anterior cardinal vein; CCV, common cardinal vein; PCV, posterior cardinal vein; SV, sinus venosus; III/IV/VI, 3/4/6th pharyngeal arch artery; LB, lung bud; B, Bronchus; yellow arrowhead, pulmonary vein; yellow arrow, pulmonary artery. Bar = 200 μm.

4. Discussion

4.1. Spatio-temporal development of the pulmonary venous return is divided into three stages

Rammos et al. divided the PV development into three main stages: the peripheral (or precirculatory), intermediate and central drainage periods (Rammos et al., 1990). These terms are useful for distinguishing the peripheral and central origin of PV malformation observed in human anomalies. According to their definitions, the peripheral drainage stage shows no obvious microscopically detectable connections between the primitive atrium and developing lung. The authors found that mouse embryos at E7.8–8.8 had no central drainage but did have peripheral drainage. The embryos stained in the current study showed no detectable splanchnic plexus, primitive PVs and peripheral returns at E8.5. These strands were first detected osculating the plexus at E9.0. The expression patterns did not depict the formation of peripheral strands before that of the primitive PV strand, and most of the strands and the plexus were not canalized at these stages. Therefore, we defined these stages as precirculatory stages.

The mechanisms underlying vascular development are heterogeneous and remain elusive, depending on the blood flow, local demands for oxygen/nutrients and genetic regulation (Isogai et al., 2003, 2001). Ablation of the blood flow disrupts the modification of the primary formed vascular network, but genetic pathways necessary for the primary vascular formation and its modification have also been identified (Lawson et al., 2002; Mukouyama et al., 2002). During PV development, several genetic factors have been shown to regulate the number and location of the vein (Burns et al., 2019; Degenhardt et al., 2013). Our spatiotemporal analyses utilizing molecular markers support the notion of blood flow-independent regulation, given that the primary vascular meshwork, including the strands connecting the aortic circulation to the systemic veins and sinoatrial segment, is established prior to the blood flow supply. During the peripheral and intermediate stages, returns to the systemic venous tributaries were observed, immediately followed by the opening of the central PV return. After the establishment of the central drainage, the peripheral pathways decline gradually. The secondary modification and canalization of the plexus and its drainage pathway might depend on such hemodynamics, e.g. shear stress, which may be greater at this stage compared to the precirculatory stage (Campinho et al., 2020).

4.2. The early expression of Emcn, CD31 and Flk1 in splanchnic plexus development possibly followed by CD34

It has been suggested that vascular endothelial cells are heterogenous following the context of the individual organs or pathological conditions (Géraud et al., 2012; Hennigs et al., 2021). Even the CD31, which shows the most homogenous expression in the adult organs, shows context dependent expression profiles (Pusztaszeri et al., 2006).

Such studies concerning the diversity of the endothelial cell in marker expressions have been conducted primarily in the adult tissues, meanwhile, few studies on developing vascular tree of embryos are reported systematically.

Our results suggested that the CD31 and Emcn are the best early markers to depict the splanchnic plexus development. CD31 was originally identified as a major endothelial cell adhesion molecule, and its expression is the most common molecular feature of the endothelial cells in all context including embryogenesis (Pusztaszeri et al., 2006; Walls et al., 2008). Emcn is a transmembrane sialomucin that is specifically expressed on the capillary and venous endothelium (Morgan et al., 1999; Park-Windhol et al., 2017; Samulowitz et al., 2002). In mouse embryos, the expression of Emcn is first observed at E8.0 in all embryonic vessels detectable at this stage, except for the yolk sac (Brachtendorf et al., 2001). After the earliest stages of embryonic vascular development, arterial endothelial cells lose their Emcn expression but show strong arterial CD31 immunostaining, which also facilitates the identification of arteries in relation to other vessel types within the skeletal system (Watson and Adams, 2018). Some previous reports used a mixture of CD31 and Emcn to detect all vessels in early development, while Emcn seems to be the first choice for observations during cardiac development (Havrilak et al., 2017). Although such differences in expression between CD31 and Emcn have been observed in early embryogenesis, their expression profiles were identical during pulmonary vascular system development.

CD34 is a endothelial sialomucin closely related with Emcn in its structure (Matsubara et al., 2005). They have been reported to show similar expression pattern during early embryogenesis, although the anti-CD34 staining are much weaker in sagittal and transverse sections of the embryos (Brachtendorf et al., 2001). In the current study, the expression of Emcn is dominant in the developing pulmonary and systemic vessels compared to the CD34. Emcn, but not CD34, is indicated to regulate the VEGF signaling regulating endothelial call proliferation, migration and survival (Hu et al., 2020; Nielsen and McNagny, 2008). Although the molecular mechanisms to establish the systemic and central drainage pathways of the future pulmonary plexus have not been revealed yet, the heterogenous character of the endothelial cells contributing the drainage pathways might be reflected by the different expression patterns of the maker molecules. Further investigation will tell whether the difference in their expression indicate the specific endothelial cell character contributing to the differentiation of the splanchnic plexus.

Flk1, also known as VEGFR2, is a tyrosine kinase receptor for VEGFA, and its expression is detected in early developing endothelial cells but not in mature ones (Yamaguchi et al., 1993). The Flk1-GFP mouse used in the present study recapitulates the endogenous expression of Flk1 and serves as a surrogate marker of the developing endothelial cells (Ishitobi et al., 2010; Okabe et al., 2014). Consistent with these previous reports, the Flk1 expression was detected just prior to the onset of blood entry in the splanchnic plexus.

The present study showed that the formation of the splanchnic plexus was depicted firstly by Emcn and CD31 expression, rather than CD34. Furthermore, the primitive returns of the plexus to the peripheral and central venous systems was depicted well by all the marker molecules investigated.

4.3. Origin of the PV orifice

The splanchnic plexus develops its venous strands connecting to the SV and sinoatrial region prior to the lung bud formation (Brown, 1913; Rammos et al., 1990; Sizarov et al., 2010). According to the topological structure depicted by our data, this is feasible, as the SV and sinoatrial region are the closest venous system within the mediastinal mesenchyme. Our observations using Emcn antibody support the notion of a blood flow-independent primitive PV formation, as discussed above; however, the topological features of the immature plexus and adjacent sinoatrial region should be noted. Whether the orifice of the primitive PV is formed in the atrium or SV has long been debated (Auër, 1948; Butler, 1952; Tasaka et al., 1996; Webb et al., 1998). Although the myocardial walls of the systemic venous sinus and PV reportedly have distinct lineages (mouse: Christoffels et al., 2006; Mommersteeg et al., 2007, human: Sizarov et al., 2010), it is worth considering that the endothelia excavating the drainage pathway of gastrorespiratory primordia firstly open into the sinoatrial region following the basic character of the endothelia, as observed in the systemic venous return formation. Sizarov et al. suggested that the luminal endothelia and the surrounding mesenchyme be considered independently (Sizarov et al., 2010). Our topological observation supports the notion that the lumen of the venous pole develops as a main systemic venous structure, as suggested previously.

4.4. The progression of the splanchnic plexus to the pulmonary plexus in the absence of the lung bud

The splanchnic plexus was firstly observed at E9.0 and expanded cranially forming future pulmonary plexus at E9.5. At this time point, the structure of the respiratory system was just a groove or a diverticulum. Although the pulmonary plexus eventually contributes to the peripheral vascular system of the lung, its formation is accompanied by the primitive respiratory anlage. Furthermore, the pulmonary pit, which is the future pulmonary vein and contributes to the central vascular system in lung, was also observed prior to the formation of the lung bud. This observation is consistent with the previous report (Peng et al., 2013). These results may suggest that the primitive respiratory anlage might have some functions for the progression of the splanchnic plexus to the pulmonary plexus and PV induction in the absence of lung buds. Further studies, e.g. ablating the early respiratory anlage, are necessary to elucidate their precise dependency.

In conclusion, the present study compared the expression of commonly used cytoplasmic endothelial cell markers during pulmonary vascular system development. Furthermore, this is the first study describing the cellular dynamics of endothelia during the early stages of respiratory organ development based on the molecular marker expressions. Our findings provide important clues for histological analyses concerning the discrete circulation development and novel insights for furthering our understanding of the embryological etiology of heart disease, such as APVR.

CRediT authorship contribution statement

Shizuka Abe: Conceptualization, Methodology, Investigation, Writing – original draft. **Aki Murashima:** Conceptualization, Methodology, Investigation, Writing – review & editing, Funding acquisition. **Eiji Kimura:** Writing – review & editing. **Masatsugu Ema:** Resources. **Jiro Hitomi:** Writing – review & editing, Supervision.

Conflicts of Interest

The authors declare no conflicts of interest associated with this manuscript.

Acknowledgements

This work was supported by JSPS KAKENHI Grant Numbers JP17K08495 and JP 20K07229. We thank Ms. Oikawa S for her great technical supports.

Appendix A. Supporting information

Supplementary data associated with this article can be found in the online version at doi:10.1016/j.acthis.2021.151840.

References

Auër, J., 1948. The development of the human pulmonary vein and its major variations. Anat. Rec. 101 (4), 581–594. https://doi.org/10.1002/ar.1091010407.

van den Berg, G., Moorman, A.F.M., 2011. Development of the pulmonary vein and the systemic venous sinus: an interactive 3D overview. PLoS One 6, e22055. https://doi.org/10.1371/journal.pone.0022055.

Blom, N.A., Gittenberger-de Groot, A.C., Jongeneel, T.H., DeRuiter, M.C., Poelmann, R. E., Ottenkamp, J., 2001. Normal development of the pulmonary veins in human embryos and formulation of a morphogenetic concept for sinus venosus defects. Am. J. Cardiol. 87 (3), 305–309. https://doi.org/10.1016/S0002-9149(00)01363-1.

de Boer, B.A., van den Berg, G., de Boer, P.A.J., Moorman, A.F.M., Ruijter, J.M., 2012. Growth of the developing mouse heart: an interactive qualitative and quantitative 3D atlas. Dev. Biol. 368 (2), 203–213. https://doi.org/10.1016/j.ydbio.2012.05.001.

Brachtendorf, G., Kuhn, A., Samulowitz, U., Knorr, R., Gustafsson, E., Potocnik, A.J., Fässler, R., Vestweber, D., 2001. Early expression of endomucin on endothelium of the mouse embryo and on putative hematopoietic clusters in the dorsal aorta. Dev. Dyn. 222 (3), 410–419. https://doi.org/10.1002/dvdy.1199.

Brown, A.J., 1913. The development of the pulmonary vein in the domestic cat. Anat. Rec. 7 (9), 299–330. https://doi.org/10.1002/ar.1090070903.

Brune, R.M., Bard, J.B.L., Dubreuil, C., Guest, E., Hill, W., Kaufman, M., Stark, M., Davidson, D., Baldock, R.A., 1999. A three-dimensional model of the mouse at embryonic day 9. Dev. Biol. 216 (2), 457–468. https://doi.org/10.1006/dbio.1999.9500.

Burns, T.A., Deepe, R.N., Bullard, J., Phelps, A.L., Toomer, K.A., Hiriart, E., Norris, R.A., Haycraft, C.J., Wessels, A., 2019. A novel mouse model for cilia-associated cardiovascular anomalies with a high penetrance of total anomalous pulmonary venous return. Anat. Rec. 302 (1), 136–145. https://doi.org/10.1002/ar.23909.

Butler, H., 1952. Some derivatives of the foregut venous plexus of the albino rat, with reference to man. J. Anat. 86 (2), 95–109.

Campinho, P., Vilfan, A., Vermot, J., 2020. Blood flow forces in shaping the vascular system: a focus on endothelial cell behavior. Front. Physiol. 11.552 https://doi.org/10.3389/fphys.2020.00552.

Christoffels, V.M., Mommersteeg, M.T.M., Trowe, M.O., Prall, O.W.J., De Gier-De Vries, C., Soufan, A.T., Bussen, M., Schuster-Gossler, K., Harvey, R.P., Moorman, A.F. M., Kispert, A., 2006. Formation of the venous pole of the heart from an Nkx2-5-negative precursor population requires Tbx18. Circ. Res. 98 (12), 1555–1563. https://doi.org/10.1161/01.RES.0000227571.84189.65.

Degenhardt, K., Singh, M.K., Aghajanian, H., Massera, D., Wang, Q., Li, J., Li, L., Choi, C., Yzaguirre, A.D., Francey, L.J., Gallant, E., Krantz, I.D., Gruber, P.J., Epstein, J.A., 2013. Semaphorin 3d signaling defects are associated with anomalous pulmonary venous connections. Nat. Med. 19 (6), 760–765. https://doi.org/10.1038/nm.3185.

DeRuiter, M.C., Gittenberger-de Groot, A.C., Poelmann, R.E., VanIperen, L., Mentink, M. M.T., 1993. Development of the pharyngeal arch system related to the pulmonary and bronchial vessels in the avian embryo: With a concept on systemic-pulmonary collateral artery formation. Circulation 87 (4), 1306–1319. https://doi.org/10.1161/01.CIR.87.4.1306.

Géraud, C., Evdokimov, K., Straub, B.K., Peitsch, W.K., Demory, A., Dörflinger, Y., Schledzewski, K., Schmieder, A., Schemmer, P., Augustin, H.G., Schirmacher, P., Goerdt, S., 2012. Unique cell type-specific junctional complexes in vascular endothelium of human and rat liver sinusoids. PLoS One 7, e34206. https://doi.org/10.1371/journal.pone.0034206.

Hasegawa, S., Susaki, E.A., Tanaka, T., Komaba, H., Wada, T., Fukagawa, M., Ueda, H.R., Nangaku, M., 2019. Comprehensive three-dimensional analysis (CUBIC-kidney) visualizes abnormal renal sympathetic nerves after ischemia/reperfusion injury. Kidney Int. 96 (1), 129–138. https://doi.org/10.1016/j.kint.2019.02.011.

Havrilak, J.A., Melton, K.R., Shannon, J.M., 2017. Endothelial cells are not required for specification of respiratory progenitors. Dev. Biol. 427 (1), 93–105. https://doi.org/10.1016/j.ydbio.2017.05.003.

Hennigs, J.K., Matuszcak, C., Trepel, M., Körbelin, J., 2021. Vascular endothelial cells: Heterogeneity and targeting approaches. Cells 10 (10), 2712. https://doi.org/10.3390/cells10102712.

His, W., 1880. Die area interposita, die Eustachische klappe und die spina vestibuli. Anat. Menschl. Embryonen 149–152.

Hu, Z., Cano, I., Saez-Torres, K.L., LeBlanc, M.E., Saint-Geniez, M., Ng, Y.S., Argüeso, P., D'Amore, P.A., 2020. Elements of the endomucin extracellular domain essential for VEGF-induced VEGFR2 activity. Cells 9 (6), 1413. https://doi.org/10.3390/cells9061413.

Ishitobi, H., Matsumoto, K., Azami, T., Itoh, F., Itoh, S., Takahashi, S., Ema, M., 2010. Flk1-GFP BAC Tg mice: an animal model for the study of blood vessel development. Exp. Anim. 59 (5), 615–622. https://doi.org/10.1538/expanim.59.615.

Isogai, S., Horiguchi, M., Weinstein, B.M., 2001. The vascular anatomy of the developing zebrafish: an atlas of embryonic and early larval development. Dev. Biol. 230 (2), 278–301. https://doi.org/10.1006/dbio.2000.9995.

Isogai, S., Lawson, N.D., Torrealday, S., Horiguchi, M., Weinstein, B.M., 2003. Angiogenic network formation in the developing vertebrate trunk. Development 130 (21), 5281–5290. https://doi.org/10.1242/dev.00733.

Lawson, N.D., Vogel, A.M., Weinstein, B.M., 2002. Sonic hedgehog and vascular endothelial growth factor act upstream of the Notch pathway during arterial endothelial differentiation. Dev. Cell 3 (1), 127–136. https://doi.org/10.1016/S1534-5807(02)00198-3.

Matsubara, A., Iwama, A., Yamazaki, S., Furuta, C., Hirasawa, R., Morita, Y., Osawa, M., Motohashi, T., Eto, K., Ema, H., Kitamura, T., Vestweber, D., Nakauchi, H., 2005. Endomucin, a CD34-like sialomucin, marks hematopoietic stem cells throughout development. J. Exp. Med. 202 (11), 1483–1492. https://doi.org/10.1084/jem.20051325.

Mommersteeg, M.T.M., Brown, N.A., Prall, O.W.J., De Gier-De Vries, C., Harvey, R.P., Moorman, A.F.M., Christoffels, V.M., 2007. Pitx2c and Nkx2-5 are required for the formation and identity of the pulmonary myocardium. Circ. Res. 101 (9), 902–909. https://doi.org/10.1161/CIRCRESAHA.107.161182.

Morgan, S.M., Samulowitz, U., Darley, L., Simmons, D.L., Vestweber, D., 1999. Biochemical characterization and molecular cloning of a novel endothelial-specific sialomucin. Blood 93 (1), 165–175. https://doi.org/10.1182/blood.v93.1.165.

Mukouyama, Y.S., Shin, D., Britsch, S., Taniguchi, M., Anderson, D.J., 2002. Sensory nerves determine the pattern of arterial differentiation and blood vessel branching in the skin. Cell 109 (6), 693–705. https://doi.org/10.1016/S0092-8674(02)00757-2.

Murashima, A., et al., 2011. Essential roles of androgen signaling in Wolffian duct stabilization and epididymal cell differentiation. Endocrinology 152 (4), 1640–1651. https://doi.org/10.1210/en.2010-1121.

Nielsen, J.S., McNagny, K.M., 2008. Novel functions of the CD34 family. J. Cell Sci. 121 (22), 3683–3692. https://doi.org/10.1242/jcs.037507.

Okabe, K., Kobayashi, S., Yamada, T., Kurihara, T., Tai-Nagara, I., Miyamoto, T., Mukouyama, Y.S., Sato, T.N., Suda, T., Ema, M., Kubota, Y., 2014. Neurons limit angiogenesis by titrating VEGF in retina. Cell 159 (3), 584–596. https://doi.org/10.1016/j.cell.2014.09.025.

Park-Windhol, C., Ng, Y.S., Yang, J., Primo, V., Saint-Geniez, M., D'amore, P.A., 2017. Endomucin inhibits VEGF-induced endothelial cell migration, growth, and morphogenesis by modulating VEGFR2 signaling. Sci. Rep. 7 (1), 17138. https://doi.org/10.1038/s41598-017-16852-x.

Peng, T., Tian, Y., Boogerd, C.J., Lu, M.M., Kadzik, R.S., Stewart, K.M., Evans, S.M., Morrisey, E.E., 2013. Coordination of heart and lung co-development by a multipotent cardiopulmonary progenitor. Nature 500 (7464), 589–592. https://doi.org/10.1038/nature12358.

Pusztaszeri, M.P., Seelentag, W., Bosman, F.T., 2006. Immunohistochemical expression of endothelial markers CD31, CD34, von Willebrand factor, and Fli-1 in normal human tissues. J. Histochem. Cytochem. 54 https://doi.org/10.1369/jhc.4A6514.2005.

Rammos, S., Gittenberger-de Grott, A.C., Oppenheimer-Dekker, A., 1990. The abnormal pulmonary venous connexion: a developmental approach. Int. J. Cardiol. 29 (3), 285–295. https://doi.org/10.1016/0167-5273(90)90116-M.

Rasband, W.S., 1997. ImageJ, U. S. National Institutes of Health, Bethesda, Maryland, USA [WWW Document]. URL ⟨http://imagej.nih.gov/ij/⟩ (accessed 6 February 2021).

Samulowitz, U., Kuhn, A., Brachtendorf, G., Nawroth, R., Braun, A., Bankfalvi, A., Böcker, W., Vestweber, D., 2002. Human endomucin: distribution pattern, expression on high endothelial venules, and decoration with the MECA-79 epitope. Am. J. Pathol. 160 (5), 1669–1681. https://doi.org/10.1016/S0002-9440(10)61114-5.

Savolainen, S.M., Foley, J.F., Elmore, S.A., 2009. Histology atlas of the developing mouse heart with emphasis on E11.5 to E18.5. Toxicol. Pathol. 37 (4), 395–414. https://doi.org/10.1177/0192623309335060.

Schneider, C.A., Rasband, W.S., Eliceiri, K.W., 2012. NIH Image to ImageJ: 25 years of image analysis. Nat. Methods 9 (7), 671–675. https://doi.org/10.1038/nmeth.2089.

Shaner, R.F., 1961. The development of the bronchial veins, with special reference to anomalies of the pulmonary veins. Anat. Rec. 140 (3), 159–165. https://doi.org/10.1002/ar.1091400302.

Sizarov, A., Anderson, R.H., Christoffels, V.M., Moorman, A.F.M., 2010. Three-dimensional and molecular analysis of the venous pole of the developing human heart. Circulation 122 (8), 798–807. https://doi.org/10.1161/CIRCULATIONAHA.110.953844.

Tasaka, H., Krug, E.L., Markwald, R.R., 1996. Origin of the pulmonary venous orifice in the mouse and its relation to the morphogenesis of the sinus venosus, extracardiac mesenchyme (spina vestibuli), and atrium. Anat. Rec. 246 (1), 107–113. https://doi.org/10.1002/(SICI)1097-0185(199609)246:1<107::AID-AR12>3.0.CO;2-T.

Theiler, K., 1989b. The House Mouse: Atlas of Embrionic Development, first ed. Springer-Verlag Berlin Heidelberg, New York.

Walls, J.R., Coultas, L., Rossant, J., Henkelman, R.M., 2008. Three-dimensional analysis of vascular development in the mouse embryo. PLoS One 3, e2853. https://doi.org/10.1371/journal.pone.0002853.

Watson, E.C., Adams, R.H., 2018. Biology of bone: the vasculature of the skeletal system. Cold Spring Harb. Perspect. Med. 8 (7), a031559 https://doi.org/10.1101/cshperspect.a031559.

Webb, S., Brown, N.A., Wessels, A., Anderson, R.H., 1998. Development of the murine pulmonary vein and its relationship to the embryonic venous sinus. Anat. Rec. 250 (3), 325–334. https://doi.org/10.1002/(SICI)1097-0185(199803)250:3<325::AID-AR7>3.0.CO;2-Z.

Wessels, A., Anderson, R.H., Markwald, R.R., Webb, S., Brown, N.A., Viragh, S., Moorman, A.F.M., Lamers, W.H., 2000. Atrial development in the human heart: an immunohistochemical study with emphasis on the role of mesenchymal tissues. Anat. Rec. 259 (3), 288–300. https://doi.org/10.1002/1097-0185(20000701)259:3<288::AID-AR60>3.0.CO;2-D.

Yamaguchi, T.P., Dumont, D.J., Conlon, R.A., Breitman, M.L., Rossant, J., 1993. Flk-1, an fit-related receptor tyrosine kinase is an early marker for endothelial cell precursors. Development 118, 489–498.

Yamamoto, Y., Shiraishi, I., Dai, P., Hamaoka, K., Takamatsu, T., 2007. Regulation of embryonic lung vascular development by vascular endothelial growth factor receptors, Flk-1 and Flt-1. Anat. Rec. 290 (8), 958–973. https://doi.org/10.1002/ar.20564.